

Journal of Mechanics of Materials and Structures

**EDGE STIFFNESS EFFECTS ON THIN-FILM LAMINATED DOUBLE GLAZING
SYSTEM DYNAMICAL BEHAVIOR BY THE OPERATIONAL MODAL ANALYSIS**

Ali Akrouf, Mariem Miladi Chaabane, Lotfi Hammami and Mohamed Haddar

Volume 7, No. 8-9

October 2012



EDGE STIFFNESS EFFECTS ON THIN-FILM LAMINATED DOUBLE GLAZING SYSTEM DYNAMICAL BEHAVIOR BY THE OPERATIONAL MODAL ANALYSIS

ALI AKROUT, MARIEM MILADI CHAABANE, LOTFI HAMMAMI AND MOHAMED HADDAR

We apply operational modal analysis (OMA) to determine the eigenfrequencies and the eigenmode shapes of a thin-film laminated double glazing system. For this purpose, the dynamic behaviors of both a laminate alone and a coupled system (double-wall structure) for specific boundary conditions are investigated. Here, the laminated plate which is composed of two elastic skins joined with an adhesive ultra-thin film is bonded by an elastic joint. Thus, two configurations of the thin-film laminated glass plate elastic boundary conditions are considered. The first one assumes that the structure is bonded by a translational stiffness (linear springs). In the second one, besides the translational stiffness, a rotational stiffness (angular springs) is introduced in order to improve the developed model. The modal recombination results of a thin-film laminated glass plate as well as those of the thin-film laminated double glazing system are presented and compared to the estimated modes achieved by OMA. Since a good agreement is obtained, the OMA technique can be used to determine the modal parameters by considering the experimental vibratory responses of the studied system. In addition, the vibration's amplitude of two laminated glass plates linked from edge to edge with both linear and angular springs can be much reduced compared to the one of the same structure bonded only by linear springs.

1. Introduction

In recent years, several structural damping calculations have been carried out in order to control vibration amplitudes and sound transmissions through windows. Thus, as presented in works such as [Antonio et al. 2003] and [Cheng et al. 2005], double panel systems offers improved vibro-acoustic behaviors and can be used in building constructions, medication equipments, automobiles and aeronautical industries. In fact, to calculate the dynamic responses of a fluid-structure coupled problem, some mathematical models can be mixed. In this context, Bouhioui [1993] combined a finite element model with an integral equation formulation in order to determine the sound transmission loss through an elastic double glazing system. This model is recently improved by Basten et al. [2001] who developed an acousto-elastic model for a double elastic panel in which the viscothermal fluid cavity effects are taken into account. Besides, in [Akrouit et al. 2008b; 2009; 2010], a structural damping model of simple and laminated plates is coupled to the viscothermal fluid model developed by Basten et al. in order to obtain a new configuration of fluid-structure coupled system. In this case, the classical modal analysis is mixed with an iterative procedure in order to calculate the vibro-acoustic modes.

Furthermore, the lamination effects give more damping to a considered vibrating panel excited by mechanical force and/or acoustical pressure; see for example [Zenkert 1995; Reddy 1997; Khdeir and

Keywords: thin-film laminated double glazing, rotational stiffness, translational stiffness, operational modal analysis, blind source separation, eigenmodes.

Reddy 1999; Carrera 2004]. In this context, Assaf [1991] analyzed the dynamic effects of a viscoelastic core on standard sandwich plate vibratory behavior by taking into account essentially the shearing work in the core and the coupling between membranous and bending effects. In the same context, Abdennadher et al. [2005b] developed a dynamic model in order to characterize the modal damping induced by a double sandwich panels. Recently, Akrouit et al. [2008a] showed that the lamination process based on ultra-thin film at the skin's interface let's to provide reduced plate's deflection amplitudes. Additionally, stiffness boundary conditions have considerable effects on dynamic responses of plates. In fact, the study of a double panel system dynamic behavior for various boundary conditions have been carried out by many researchers; see for example [Abbès et al. 2011; Abdennadher et al. 2005a]. Then, if a damping and/or a stiffness of plate edge is considered, the vibro-acoustic responses amplitude can be much reduced. For this purpose, Park et al. [2003] examined the effect of viscoelastic supports at the level of plate's edges. It has been shown that the plate's velocity and the sound energy are effectively affected by the damping on the level of the edges inducing reduced vibration amplitudes. Also, Vallaban et al. [1997] considered a structural joint at the level of a glass panel edges. It has been concluded that the dynamic behavior of the plate-joint can be improved by increasing the stress in the joint produced by the shearing forces on the level of the edges.

As a resolution method, we can use especially the Operational Modal Analysis (OMA) formulation which has been previously established by many researchers in neuroscience and signal processing; see for example [Hérault and Ans 1984; 1985; Nguyen et al. 1994]. In this context, independent component analysis, one of the major techniques of the BSS method, can be exploited in order to solve BSS problems in the case of linear or nonlinear convolutive mixtures as presented in [Zarzoso and Comon 2008; Antoni et al. 2004; 2005]. This method needs to know only the sensor's measurement or the FE vibratory responses in order to estimate the eigenfrequencies of a studied structure. It's defined by a separation procedure applied on independent linear mixture signal by using only the measured vibratory response of the system. Poncelet et al. [2007] used ICA in order to exploit the virtual source theory by studying an output-only modal analysis. Kerschen et al. [2007] used the modal assurance criterion to establish the relation between exact and estimated modes. In this work, the OMA method is presented and exploited in order to extract the eigenmodes of a thin-film laminated double glazing system with elastic boundary conditions. In this case, both translational and rotational stiffness are considered at the level of the plate's edges. The model validation is obtained by comparing the exact (numerical) and estimated eigenfrequencies of a thin-film laminated glass plate for two cases of elastic boundary conditions: the first model assumes that the laminated plate is fixed only by a linear springs. In the second one, the same structure is fixed by both linear and angular springs. Moreover, the dynamic responses of each case are presented and discussed. Also, the exact and estimated eigenmodes shapes of a thin-film laminated double glazing system are presented and compared. Thus, the influence of the system's edge stiffness can be analyzed.

2. Mathematical formulation

2.1. The OMA method. As presented in [Hérault and Ans 1984; 1985; Nguyen et al. 1994], the operational modal analysis (OMA) method is based on independent component analysis (ICA), a recent approach used in signal treatment. We briefly describe the setup. Consider N_s source signals emitted

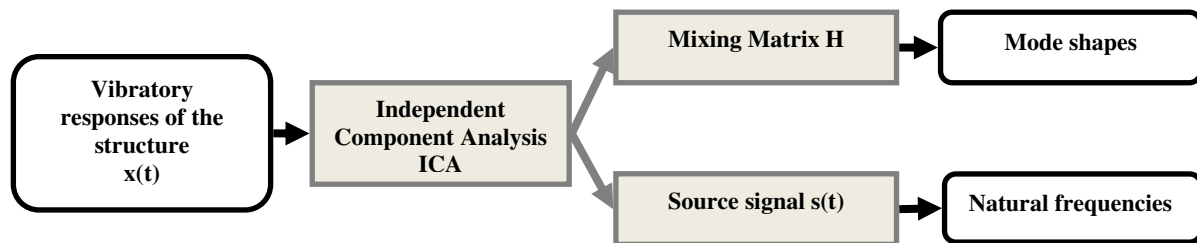


Figure 1. Separation procedure: ICA concept.

through a dynamic system modeled by a mixture matrix of dimension $N_s \times N_c$ and received by N_c sensors. Then, the model equation can be expressed as (see [Abbès et al. 2011; Zarzoso and Comon 2008; Poncelet et al. 2007])

$$x_i = \sum_{j=1}^{N_s} h_{ij}s_j + b_i, \quad i = 1, \dots, N_c. \quad (1)$$

Equation (1) can be written in matrix form as

$$\{x\} = [H]\{s\} + \{b\}, \quad (2)$$

where $\{x\} = \langle x_1, \dots, x_{N_c} \rangle^T$ represents the N_c observations vector, $\{s\} = \langle s_1, \dots, s_{N_s} \rangle^T$ represents the N_s signals sources vector, $[H] = [\{h_1\}, \dots, \{h_{N_s}\}]$ is the mixture matrix of dimension $N_c \times N_s$, $\{h_j\} = \langle h_{1j}, \dots, h_{N_cj} \rangle^T$, $j = 1, \dots, N_s$, is the j -th column vector of the mixture matrix $[H]$, $\{b\}$ is a possible additive noise.

When ICA is applied in OMA, the structure physical responses defined as virtual sources with different spectral contents can be interpreted. In this case, ICA provides the mixing matrix and the modal response of the structure (Figure 1).

The dynamic response of a given mechanical system can be obtained by the modal recombination method as (see [Akrouit et al. 2008a; Abbès et al. 2011])

$$\{x\} = [\Psi]\{y\}, \quad (3)$$

where $\{x\}$ is the measured nodal vector, $[\Psi]$ represents the modal matrix and $\{y\}$ is the vector containing the modal responses. Then, by using only the output signal $\{x\}$, OMA is carried out in order to determine the eigenmode shapes existing in the modal matrix $[\Psi]$ and the eigenfrequencies contained in the modal response vector $\{y\}$.

2.2. Thin-film laminated plate dynamic model. As presented in Figure 2, the kinematical behavior of the laminate is based on the theory that introduce a specific behavior law for an ultra-thin adhesive film of stiffness k_{film} confined at the interface of two skin plies of thicknesses (h_1, h_2) which satisfy for the Kirchhoff plate's theory. In this case, ℓ_x and ℓ_y are the half dimensions of the laminate with respect to directions x and y .

Then, the vibratory behavior of the laminated glass plate is described by both dynamics of skins and the ultra-thin adhesive film.

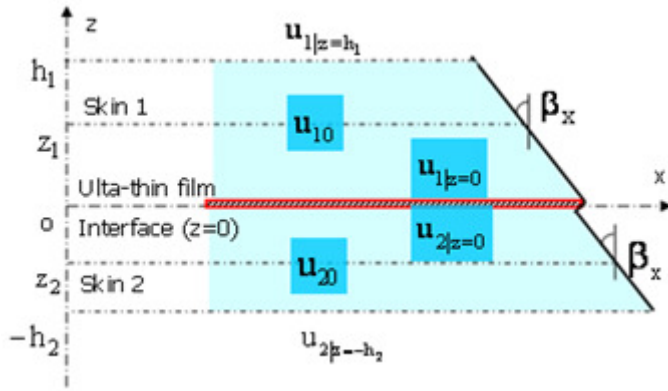


Figure 2. In plane (x, z) thin-film laminate kinematic model.

Consequently, the displacement field in the thin-film laminated glass plate can be expressed as follows [Akrouit et al. 2008a]:

$$x\text{-direction} : \begin{cases} u_1 = u_m + \frac{[u_\tau]}{2} + (z - z_m)\beta_x \\ u_2 = u_m - \frac{[u_\tau]}{2} + (z - z_m)\beta_x \end{cases} \quad (4)$$

$$y\text{-direction} : \begin{cases} v_1 = v_m + \frac{[v_\tau]}{2} + (z - z_m)\beta_y \\ v_2 = v_m - \frac{[v_\tau]}{2} + (z - z_m)\beta_y \end{cases} \quad (5)$$

$$z\text{-direction} : w(x, y, z) = w(x, y) \quad (6)$$

The dynamic of the ultra-thin film can be written as a function of the shear interfacial displacements with respect to directions x and y ($[u_\tau] = u_1|_{z=0} - u_2|_{z=0}$ and $[v_\tau] = v_1|_{z=0} - v_2|_{z=0}$) as follows:

$$\begin{aligned} \tau_x &= k_{\text{film}}[u_\tau] \\ \tau_y &= k_{\text{film}}[v_\tau] \end{aligned} \quad (7)$$

where (τ_x, τ_y) are the shear interfacial stresses [Akrouit et al. 2008a].

Consequently, we can use the stress-strain relations in order to determine the energy functional of the laminate as follows:

$$\vartheta_L = (E_{\text{str.}} + E_{\text{kin.}})_{\text{skins}} + E_{\text{film}} \quad (8)$$

where $(E_{\text{str.}})_{\text{skins}}$, E_{film} and $(E_{\text{kin.}})_{\text{skins}}$ are respectively the skin's strain energy, the film strain energy and the skin's kinetic energy (by neglecting inertial terms of rotations) calculated as follows [Akrouit et al.

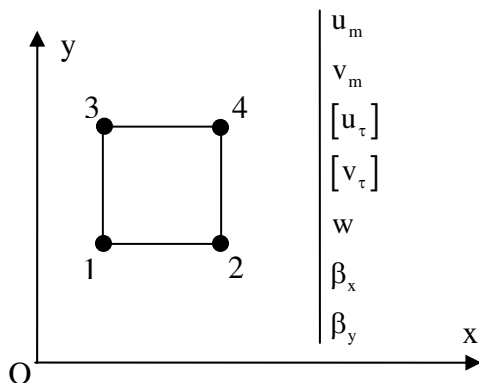


Figure 3. Laminate quadrilateral FE.

2008a]:

$$(E_{str.})_{skins} = \frac{1}{2} \int_{\Sigma} \left(\int_{-h_2}^0 \langle \sigma \rangle_2 \{ \epsilon \}_2 dz + \int_0^{h_1} \langle \sigma \rangle_1 \{ \epsilon \}_1 dz \right) d\Sigma \tag{9}$$

$$E_{film} = \frac{1}{2} \int_{\Sigma} \langle [u_{\tau}] [v_{\tau}] \rangle \begin{bmatrix} k_{film} & 0 \\ 0 & k_{film} \end{bmatrix} \begin{Bmatrix} [u_{\tau}] \\ [v_{\tau}] \end{Bmatrix} d\Sigma \tag{10}$$

$$E_{kin.} = \frac{1}{2} \sum_{i=1}^2 \int_{\Sigma} \left(\int_{-h_2}^{h_1} \rho_i (\dot{u}_i^2 + \dot{v}_i^2 + \dot{w}^2) dz \right) d\Sigma \tag{11}$$

The homogenous energy functional of the laminated glass plate can be obtained by integrating (9) and (11) with respect to z .

As sketched in Figure 3, the homogenous laminate energy functional is discretized by a four nodes linear quadrilateral finite element (FE). In this case, the laminate nodal vector at node ‘ i ’ contain seven degrees of freedom: $\{U\}_{node\ 'i'} = \langle u_m, v_m, [u_{\tau}], [v_{\tau}], w, \beta_x, \beta_y \rangle_{node\ 'i'}^T$.

The FE discretization of the thin-film laminated plate energy functional gives after minimization the following eigenmodes symmetrical matrix system:

$$([K_L] - \omega^2 [M_L]) \{U_L\} = \{0\} \tag{12}$$

where $[K_L]$ and $[M_L]$ are respectively the stiffness and mass matrices of the thin-film laminated plate. $\{U_L\}$ is the laminate nodal displacement vector.

2.3. Elastic joint model. As discussed in [Vallaban et al. 1997; Park et al. 2003; Abbès et al. 2011], the modal characteristics of a given structure (beams or plates) are strongly affected by specified boundary conditions. Then, an elastic joint model can be considered in order to confer better vibratory behavior to the thin-film laminate. So, the dynamic model developed in this work is based on both translational and rotational stiffness modeled by both linear and angular springs at the level of its edge (see Figure 4).

By taking into account the stiffness effects introduced above, the dynamic behavior law of the elastic joint can be defined via the relation between the force and displacements (translation w and rotations

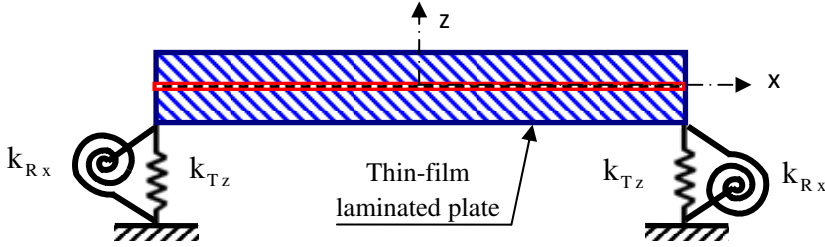


Figure 4. Thin-film laminate elastic boundary conditions.

(β_x, β_y)) at node ‘ N_i ’ of the laminate edge as follows:

$$\begin{aligned} F_{Tz \cdot Ni} &= k_{Tz} w_{Ni} \\ F_{Rx \cdot Ni} &= k_{Rx} \beta_{x \cdot Ni} \\ F_{Ry \cdot Ni} &= k_{Ry} \beta_{y \cdot Ni} \end{aligned} \tag{13}$$

Relations (13) can be written in matrix form as follows:

$$\{F_{Ni}\} = [K_{Je}]\{U_{Ni}\} \tag{14}$$

where $\{U_{Ni}\} = \langle w_{Ni} \ \beta_{x \cdot Ni} \ \beta_{y \cdot Ni} \rangle^T$ is the transversal displacement and deflection rotations vector. $\{F_{Ni}\} = \langle F_{Tz \cdot Ni} \ F_{Rx \cdot Ni} \ F_{Ry \cdot Ni} \rangle^T$ represents the force vector applied by the joint on the plate boundary. $[K_{Je}]$ is an elementary elastic joint matrix written as follows:

$$[K_{Je}] = \begin{bmatrix} k_{Tz} & 0 & 0 \\ 0 & k_{Rx} & 0 \\ 0 & 0 & k_{Ry} \end{bmatrix} \tag{15}$$

Thus, when the laminate edge contains N_n nodes, a global matrix $[K_J]$ of the elastic joint effect at the edge of the laminate can be derived as follows:

$$[K_J] = \begin{bmatrix} \begin{bmatrix} [0]_{4 \times 4} & [0]_{4 \times 3} \\ [0]_{3 \times 4} & [K_{Je}] \end{bmatrix}_{\text{node } N_1} & [0]_{7 \times 7} & \cdots & \cdots & [0]_{7 \times 7} \\ [0]_{7 \times 7} & \begin{bmatrix} [0]_{4 \times 4} & [0]_{4 \times 3} \\ [0]_{3 \times 4} & [K_{Je}] \end{bmatrix}_{\text{node } N_2} & [0]_{7 \times 7} & \cdots & [0]_{7 \times 7} \\ \vdots & [0]_{7 \times 7} & \ddots & & \vdots \\ \vdots & \vdots & & \ddots & [0]_{7 \times 7} \\ [0]_{7 \times 7} & [0]_{7 \times 7} & \cdots & [0]_{7 \times 7} & \begin{bmatrix} [0]_{4 \times 4} & [0]_{4 \times 3} \\ [0]_{3 \times 4} & [K_{Je}] \end{bmatrix}_{\text{node } N_n} \end{bmatrix} \tag{16}$$

The developed model of the elastic joint is combined with the thin-film laminated plate model allow modeling a new configuration of laminated double glazing system.

2.4. Dynamic model of a thin-film laminated double glazing system. The considered double glazing system is composed of two thin-film laminated plate bonded by the elastic joint defined in Section 2.3.

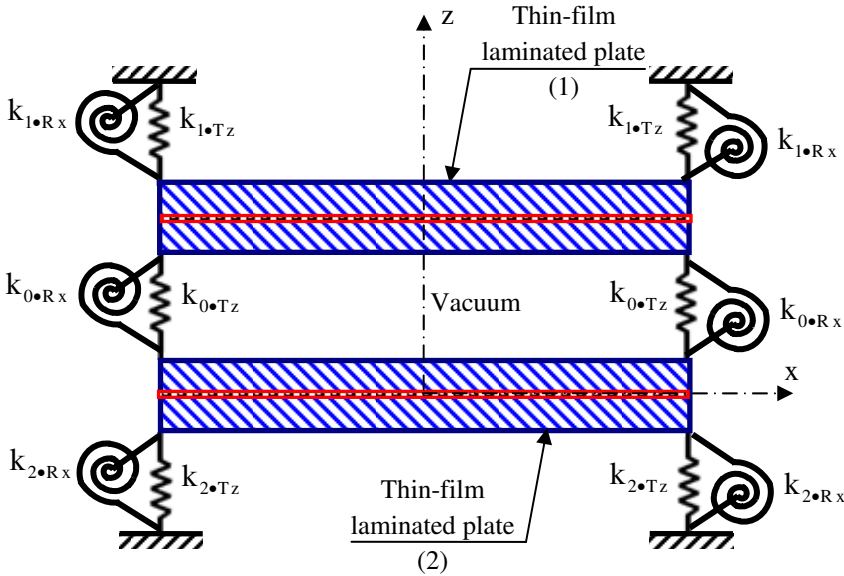


Figure 5. In plane (x, z) double laminate-joint model.

In this case, the two laminates are coupled by elastic linear and angular springs of stiffness $k_{0 \bullet T z}$ and $k_{0 \bullet R x}$. The obtained coupled system is related to a rigid body by two elastic joints ($k_{1 \bullet T z}, k_{1 \bullet R x}$) and ($k_{2 \bullet T z}, k_{2 \bullet R x}$) as presented in Figure 5.

The double glazing system energy functional can be obtained by calculating the associated energy of each part composing the system. Then, we can write:

$$\vartheta_{D.G.S} = \left(\sum_{i=1}^2 [(E_{str.} + E_{kin.})_{skins} + E_{film}]_{L_i} \right) + \left(\sum_{i=1}^2 (E_{str.})_{J_{i0}} \right) + (E_{coupling})_{J_0 \bullet L_1 \bullet L_2} \quad (17)$$

where $(E_{str.})_{J_{i0}}$ ($i = 1, 2$) and $(E_{coupling})_{J_0 \bullet L_1 \bullet L_2}$ represent respectively the strain energies due to the joint effect at the edge of the laminate L_i ($i = 1, 2$) and the laminates-joint coupling energy expressed as follows:

$$(E_{str.})_{J_{i0}} = \frac{1}{2} [(k_{0 \bullet T z} + k_{i \bullet T z}) \int_{\ell} w_i^2 d\ell + (k_{0 \bullet R x} + k_{i \bullet R x}) \int_{\ell} \beta_{xi}^2 d\ell + (k_{0 \bullet R y} + k_{i \bullet R y}) \int_{\ell} \beta_{yi}^2 d\ell] \quad (18)$$

$$(E_{coupling})_{J_0 \bullet L_1 \bullet L_2} = -\frac{1}{2} [(2k_{0 \bullet T z} \int_{\ell} w_1 w_2 d\ell) + (2k_{0 \bullet R x} \int_{\ell} \beta_{x1} \beta_{x2} d\ell) + (2k_{0 \bullet R y} \int_{\ell} \beta_{y1} \beta_{y2} d\ell)] \quad (19)$$

The discretization and the minimization of the double glazing system energy functional by the finite element method (FE) give the following symmetrical coupled matrix equation:

$$\left(\begin{bmatrix} [K_{L_1}] + [K_{J_{10}}] & -[K_{J_0 \bullet L_1 \bullet L_2}] \\ -[K_{J_0 \bullet L_1 \bullet L_2}]^T & [K_{L_2}] + [K_{J_{20}}] \end{bmatrix} - \omega^2 \begin{bmatrix} [M_{L_1}] & [0] \\ [0] & [M_{L_2}] \end{bmatrix} \right) \begin{Bmatrix} \{U_1\} \\ \{U_2\} \end{Bmatrix} = \begin{Bmatrix} \{0\} \\ \{0\} \end{Bmatrix} \quad (20)$$

where $([K_{L_1}], [K_{L_2}])$ and $([M_{L_1}], [M_{L_2}])$ represent respectively the stiffness and mass matrices of the laminates. $[K_{J_{10}}]$ and $[K_{J_{20}}]$ are respectively the stiffness matrices due to the joints effects at the edge of the laminates; obtained from the FE discretization of Equation (18) and expressed as follows:

$$\begin{aligned} [K_{J_{10}}] &= [K_{J_1}] + [K_{J_0}] \\ [K_{J_{20}}] &= [K_{J_2}] + [K_{J_0}] \end{aligned} \quad (21)$$

with: $[K_{J_0}]$, $[K_{J_1}]$ and $[K_{J_2}]$ represent respectively the stiffness matrices of the elastic joints J_0 , J_1 , and J_2 defined at the laminate boundary nodes.

$[K_{J_0 \cdot L_1 \cdot L_2}]$ is a stiffness matrix resulting from the coupling between the boundaries of two laminates (L_1, L_2) and the joint J_0 obtained from the FE discretization of Equation (19).

$\{U_1\}$ and $\{U_2\}$ represent respectively the nodal displacement vectors of laminates 1 and 2.

2.5. Modal analysis of the laminated double glazing system. The eigenmodes of the coupled system are solution of Equation (20) which can be written in the following form:

$$\begin{bmatrix} [K_{S_1}] - \omega^2[M_{S_1}] & [C_S] \\ [C_S]^T & [K_{S_2}] - \omega^2[M_{S_2}] \end{bmatrix} \begin{Bmatrix} \{U_1\} \\ \{U_2\} \end{Bmatrix} = \begin{Bmatrix} \{0\} \\ \{0\} \end{Bmatrix} \quad (22)$$

where $[K_{S_i}] = [K_{L_i}] + [K_{J_{i0}}]$, $[M_{S_i}] = [M_{L_i}]$ ($i = 1, 2$), $[C_S] = -[K_{J_0 \cdot L_1 \cdot L_2}]$.

The eigenmodes $[\Phi_{S_1}]$ and $[\Phi_{S_2}]$ of each laminate alone can be used in order to reduce the size of the coupled system (22). Then, the modal matrices of each plate alone can be written as follows:

$$[\mathbf{K}_{S_i}] = [\Phi_{S_i}]^T [K_{S_i}] [\Phi_{S_i}] = \begin{bmatrix} \ddots & & & \\ & \omega_{r \cdot S_i}^2 & & \\ & & \ddots & \\ & & & \ddots \end{bmatrix} \text{ for } \begin{cases} r = 1 \dots N_{\text{eig}} \\ i = 1, 2 \end{cases} \quad (23)$$

$$[\mathbf{M}_{S_i}] = [\Phi_{S_i}]^T [M_{S_i}] [\Phi_{S_i}] = \begin{bmatrix} \ddots & & & \\ & 1 & & \\ & & \ddots & \\ & & & \ddots \end{bmatrix} \text{ for } \begin{cases} r = 1 \dots N_{\text{eig}} \\ i = 1, 2 \end{cases} \quad (24)$$

N_{eig} represent the number of eigenmodes retained.

Consequently, the coupled matrix system (22) can be much reduced and written as follows:

$$\begin{bmatrix} \omega_{r \cdot S_1}^2 - \omega^2 & [C_S] \\ [C_S]^T & \omega_{r \cdot S_2}^2 - \omega^2 \end{bmatrix} \begin{Bmatrix} \{U_1\} \\ \{U_2\} \end{Bmatrix} = \begin{Bmatrix} \{0\} \\ \{0\} \end{Bmatrix} \quad (25)$$

where $\{U_1\}$ and $\{U_2\}$ represent, respectively the modal displacement vectors of laminates 1 and 2 defined by:

$$\begin{aligned} \{U_1\} &= [\Phi_{S_1}]^T \{U_1\} \\ \{U_2\} &= [\Phi_{S_2}]^T \{U_2\} \end{aligned} \quad (26)$$

$[C_S]$ represents the laminate-joint modal coupling matrix written as follows:

$$[C_S] = [\Phi_{S_1}]^T [C_S] [\Phi_{S_2}] \quad (27)$$

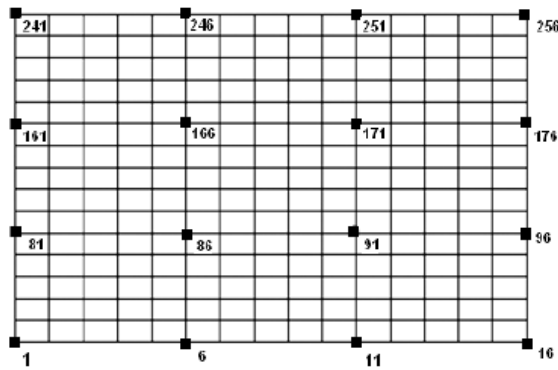


Figure 6. Laminated plate dynamic response nodes.

As discussed in [Akrouf et al. 2008b; 2009; 2010], the resolution of the coupled system (25) allows determining the coupled eigenfrequencies $\omega_{r,C}$ ($r = 1, \dots, N_{C.eig}$) and a coupled eigenmodes basis $[\Phi_C] = [\{\Phi_1\} \dots \{\Phi_{N_{C.eig}}\}]$. So, we can calculate the modal responses of the laminated double glazing system which is in free vibration and under initial excitations of the first laminate. The considered initial conditions are the following:

$$\text{for } t = 0, \begin{cases} \langle\{U_1\}\{U_2\}\rangle_{t=0} = \langle\{U_{10}\}\{0\}\rangle \\ \langle\{\dot{U}_1\}\{\dot{U}_2\}\rangle_{t=0} = \langle\{\dot{U}_{10}\}\{0\}\rangle \end{cases} \quad (28)$$

In this case, the nodal vibratory responses are obtained by the modal recombination method.

Hence, the calculated numerical responses are used as inputs in the ICA concept which is applied in the OMA method in order to obtain estimated results of the eigenfrequencies and eigenmode shapes.

3. Numerical procedure validation: case of thin-film laminated plate alone

In this part, the OMA approach is used in order to estimate the eigenmodes of a thin-film laminated glass plate alone for two cases of elastic boundary conditions:

- only a linear springs is considered at the level of the edge.
- both linear and angular springs are considered at the level of the edge.

In order to estimate the eigenfrequencies and the eigenmode shapes by the OMA method, 16 vibratory responses of the laminate x ($1, \dots, 16$) are calculated at the indicated nodes (see Figure 6). Note that, the plate is in free vibration under initial conditions.

The physical and geometrical properties of the studied structure are the following:

- skin’s laminate properties: in-plane dimensions: $\ell_x = 0.6$ m, $\ell_y = 0.4$ m, Young modulus: $E_1 = E_2 = 7.2 \times 10^4$ MPa, Poisson’s ratio: $\nu_1 = \nu_2 = 0.22$, density: $\rho_1 = \rho_2 = 2500$ Kg/m³ skin’s thickness: $h_1 = h_2 = 3$ mm.
- ultra-thin film stiffness: $k_{film} = 1.362 \times 10^7$ N/mm³ (Araldite),
- linear stiffness per length unit: $k_{Tz} = 0.264 \times 10^4$ N/m²,

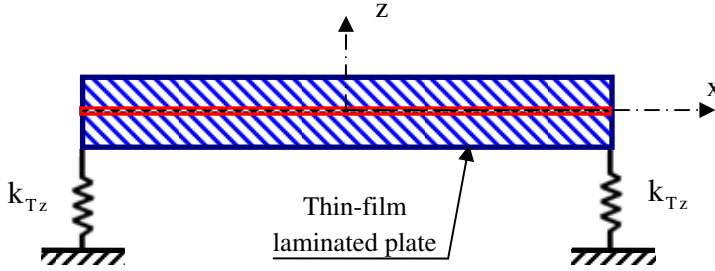


Figure 7. Laminated plate bonded by translational joint.

- angular stiffness per length unit: $k_{Rx} = k_{Ry} = 0.264 \times 10^4$ N/rad.

In the next sections, the ICA results can be compared to those obtained numerically (by the classical modal analysis). Also, the effect of angular springs added to the linear spring is presented and analyzed.

3.1. Case of translational stiffness ‘T’. In this section, the considered laminate is supported only by a translational joint as sketched in Figure 7. The laminate is supposed to be in free vibration and under arbitrary initial conditions satisfying to a standard statistical rule.

The eigenmodes of the laminate bonded by translational joint are solution of the following matrix system:

$$\begin{aligned}
 & ([[K_L] + [K_J]] - \omega^2[M_L])\{U_L\} = \{0\} \\
 & \text{for } t = 0 \begin{cases} \{U_L\} = \{U_{L0}\} \\ \{\dot{U}_L\} = \{\dot{U}_{L0}\} \end{cases} \quad (29)
 \end{aligned}$$

where $([K_L], [K_J])$ and $[M_L]$ are respectively the laminate-joint stiffness matrices and the mass matrix of the structure. $\{U_{L0}\}$ and $\{\dot{U}_{L0}\}$ are respectively the initial displacement and velocity vectors applied on the laminate.

Figure 8 presents the observed signals at nodes $x(3)$: node 11, $x(10)$: node 166, $x(12)$: node 176 and $x(14)$: node 246 which are used for the eigenmodes estimation. In analyzing the spectrum of those observed signals, we remark the existence of four dominant picks characteristics of the main natural frequencies of the laminate.

Table 1 regroups the exact and estimated eigenfrequencies of the laminated glass plate with translational boundary conditions (linear springs). The OMA results are validated by calculating the following performance criteria [Zhou and Chelidze 2007; Abbès et al. 2011]:

- The Modal Assurance Criterion defined as follows:

$$\text{MAC}_i = \frac{(\psi_i^T \bar{\psi}_i)}{(\psi_i^T \psi_i)(\bar{\psi}_i^T \bar{\psi}_i)} \quad (30)$$

where ψ_i and $\bar{\psi}_i$ are respectively the numerical (exact) and estimated eigenmodes of the laminate.

- The Euclidean distance between two vectors of the modal matrix in order to calculate the approximation error of eigenmodes as follows:

$$E_{ri} = \|\psi_i - \bar{\psi}_i\| \quad (31)$$

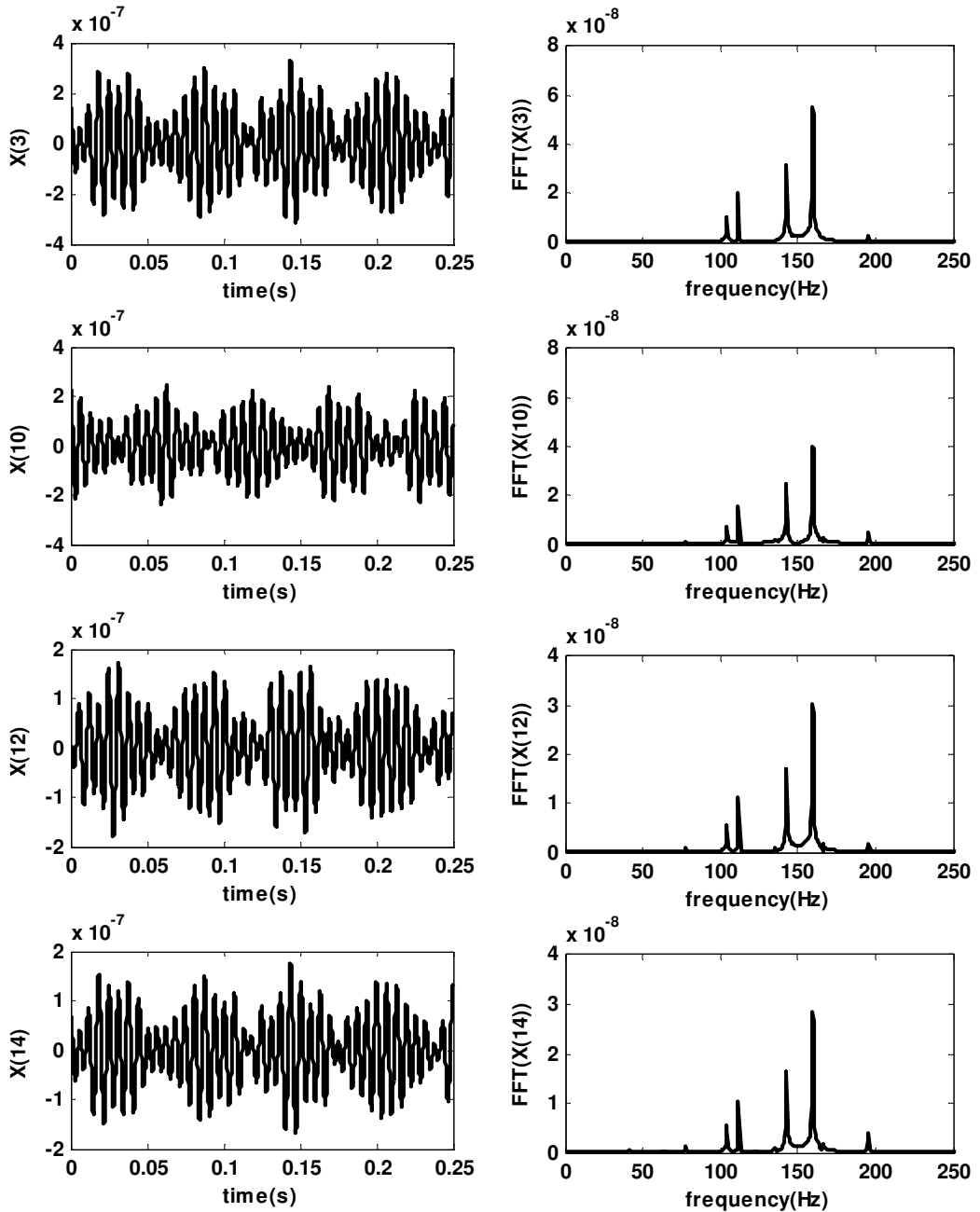


Figure 8. Some observed signals: case of laminated plate bonded by translational joint.

- The relative error E_{f_i} between the exact and estimated eigenfrequencies present good performance criteria defined as follows:

$$E_{f_i}(\%) = 100 \frac{f_i - \bar{f}_i}{f_i} \tag{32}$$

| Mode | Exact eigenfreq. (Hz) | Estimated eigenfreq. (Hz) | E_r | MAC | $E_f(\%)$ |
|------|-----------------------------|---------------------------------|--------|--------|-----------|
| 1 | 23.7771 | 24 | 0.0006 | 0.9979 | 0.9376 |
| 2 | 41.7990 | 42 | 0.0014 | 0.9996 | 0.4810 |
| 3 | 62.5867 | 62.5 | 0.0007 | 0.9999 | 0.1385 |
| 4 | 70.7569 | 71 | 0.0008 | 0.9966 | 0.3436 |
| 5 | 77.8571 | 78 | 0.0002 | 1.0000 | 0.1836 |
| 6 | 104.2231 | 104 | 0.0007 | 1.0000 | 0.2141 |
| 7 | 111.5364 | 111.5 | 0.0003 | 1.0000 | 0.0326 |
| 8 | 121.9734 | 122 | 0.0006 | 0.9998 | 0.0218 |
| 9 | 135.7371 | 135.5 | 0.0004 | 0.9999 | 0.1747 |
| 10 | 142.7350 | 142.5 | 0.0001 | 1.0000 | 0.1647 |
| 11 | 159.7369 | 159.5 | 0.0001 | 1.0000 | 0.1483 |
| 12 | 166.2010 | 166 | 0.0005 | 0.9998 | 0.1209 |
| 13 | 195.1359 | 195 | 0.0030 | 0.9557 | 0.0696 |
| 14 | 195.3606 | 195.5 | 0.0003 | 1.0000 | 0.0714 |
| 15 | 201.8061 | 202 | 0.0040 | 0.9972 | 0.0961 |
| 16 | 214.2604 | 214.5 | 0.0024 | 0.9666 | 0.1118 |

Table 1. Eigenfrequencies of a laminated plate alone bonded by translational joint.

where f_i and \bar{f}_i represent respectively the exact and estimated eigenfrequencies.

Then, the performance criteria presented in [Table 1](#) show that an excellent accord is achieved by comparing the numerical (exact) and the estimated eigenfrequencies (obtained by OMA).

As a next result, we present in [Figure 9](#) the exact and estimated eigenmode shapes for the tree first eigenfrequencies of the laminate. Hence, a good accord is obtained.

3.2. Case of both translational and rotational stiffness ‘T + R’. The model of the structure is presented in [Figure 4](#). In this case, the same nodes $\{x(3): \text{node11}, x(10): \text{node 166}, x(12): \text{node 176}$ and $x(14): \text{node 246}\}$ are used for the estimation of the laminate eigenmodes. So, according to those nodes, [Figure 10](#) present the observed signals and the corresponding spectra. In analyzing the evolution of the dynamic responses versus time, we can see a reduced vibration amplitude for the laminate fixed by both translational and rotational joints compared to the one fixed only by translational joint. Also, some eigenfrequencies have vanished in the spectrum of joint ‘R + T’ ([Figure 10](#)) compared to the spectrum of joint ‘T’ presented in [Figure 8](#).

[Table 2](#) contains the numerical and estimated eigenfrequencies of the laminated glass plate with elastic (translational and rotational) boundary conditions. The OMA results are validated by calculating the same performance criteria [[Zhou and Chelidze 2007](#); [Abbès et al. 2011](#)] defined by (30), (31) and (32). Also, the eigenfrequencies of the laminate-joint ‘R + T’ ([Table 2](#)) increased compared to those of the laminate-joint ‘T’ ([Table 1](#)). Thus, more rigidity can be conferred to the structure.

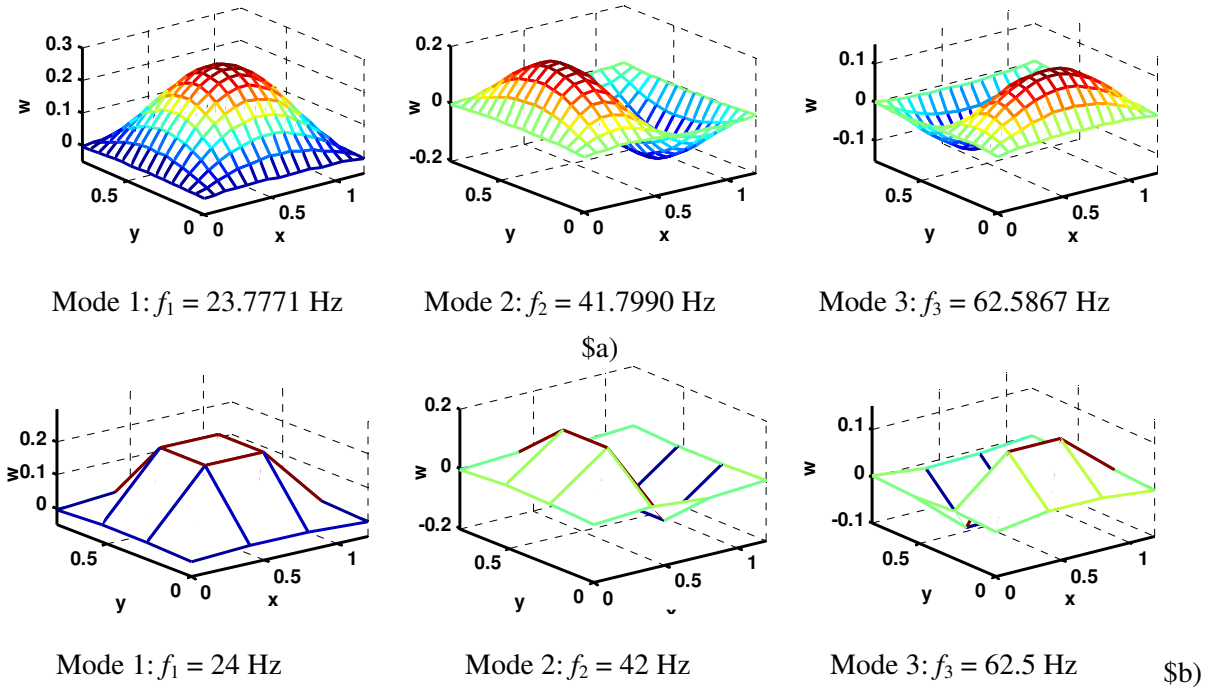


Figure 9. Eigenmode shapes of a laminated plate bonded by translational joint. (a) Exact eigenmode shapes. (b) Estimated eigenmode shapes.

In addition, Figure 11 shows the numerical (exact) and estimated eigenmode shapes of a thin-film laminated glass plate bonded by both translational and rotational joints. The same form is observed by comparing each corresponding mode presented in Figure 11(a) (exact) to the one presented in Figure 11(b) (estimated).

4. OMA application: case of thin-film laminated double glazing system

In this section, the OMA method is applied in order to identify the modal characteristics of a laminated double glazing system bonded by an elastic joint. Figure 12 presents the corresponding nodes used for the calculation of 32 vibratory responses corresponding to the coupled system.

The double glazing system is composed of two identical laminated glass plate which each one is made of two similar skins connected by an adhesive ultra-thin film.

The physical and geometrical properties of the laminate are given in Section 3.

A same elastic joint is used as boundary conditions of the coupled system (see Figure 5):

- linear stiffness per length unit: $k_{i.Tz} = k_{Tz}$, ($i = 0, 1, 2$).
- angular stiffness per length unit: $k_{i.Rx} = k_{i.Ry} = k_{Rx} = k_{Ry}$, ($i = 0, 1, 2$).

The value of k_{Tz} , k_{Rx} and k_{Ry} are given in Section 3.

In the next sections, the ICA results can be compared to those obtained numerically (by the classical modal analysis). Also, the effect of angular springs added to the linear spring is presented and analyzed.

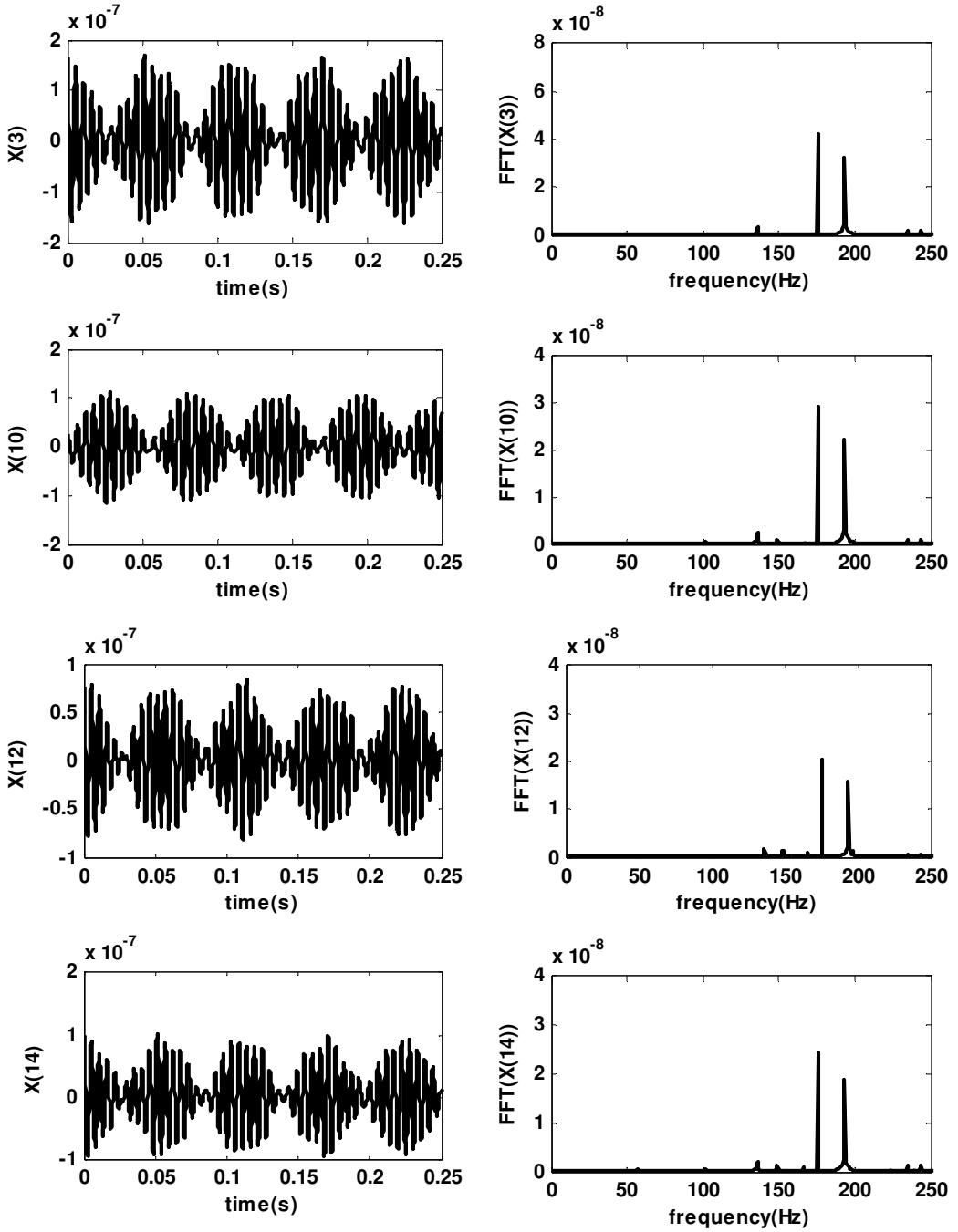


Figure 10. Some observed signals: case of laminated plate bonded by both translational and rotational joints.

| Mode | Numerical eigenfreq. (Hz) | Estimated eigenfreq. (Hz) | E_r | MAC | $E_f(\%)$ |
|------|---------------------------------|---------------------------------|--------|--------|-----------|
| 1 | 37.1843 | 37 | 0.0051 | 0.9779 | 0.4956 |
| 2 | 57.2723 | 57.5 | 0.0002 | 1.0000 | 0.3975 |
| 3 | 84.6944 | 84.5 | 0.0008 | 0.9999 | 0.2295 |
| 4 | 90.1553 | 90 | 0.0001 | 1.0000 | 0.1722 |
| 5 | 101.7795 | 102 | 0.0007 | 0.9997 | 0.2166 |
| 6 | 131.6648 | 131.5 | 0.0003 | 1.0000 | 0.1251 |
| 7 | 135.7660 | 136 | 0.0029 | 0.9999 | 0.1723 |
| 8 | 148.7430 | 149 | 0.0001 | 1.0000 | 0.1727 |
| 9 | 166.0922 | 166 | 0.0001 | 1.0000 | 0.0555 |
| 10 | 175.4942 | 175.5 | 0.0010 | 1.0000 | 0.0033 |
| 11 | 193.3816 | 193.5 | 0.0002 | 1.0000 | 0.0612 |
| 12 | 196.6265 | 196.5 | 0.0001 | 1.0000 | 0.0643 |
| 13 | 222.3098 | 222.5 | 0.0003 | 0.9999 | 0.0855 |
| 14 | 234.4725 | 234.5 | 0.0002 | 1.0000 | 0.0117 |
| 15 | 238.1860 | 238 | 0.0006 | 0.9999 | 0.0780 |
| 16 | 243.3318 | 243.5 | 0.0002 | 1.0000 | 0.0691 |

Table 2. Eigenfrequencies of a laminated plate alone bonded by both translational and rotational joints.

4.1. Observed signals of the laminated double glazing system. As observed signals, we report in the same graph (Figures 13, 14, 15 and 16) the dynamic responses of both a thin film laminated double glazing fixed by ‘T’ joint and the same system fixed by ‘R + T’ joint. These vibratory responses are determined at nodes: 166: $x(10)$ and 246: $x(14)$ for laminate 1 and at nodes: 417: $x(25)$ and 502: $x(30)$ for laminate 2.

By analyzing the vibratory responses of the laminated double glazing system with translational stiffness boundary conditions (dashed line, ‘T’) to those of the same system with both translational and rotational stiffness boundary conditions (solid line, ‘R + T’), we remark a reduced vibration amplitude for the ‘R + T’ system compared to the one for the ‘T’ system. Also, the rotational stiffness can be clearly seen in the observed signals of laminate 1 (Figures 13 and 14) on which the initial excitation conditions are applied.

4.2. Eigenfrequencies of the coupled system. Table 3 regroups the numerical (exact) and estimated (via OMA) eigenfrequencies of the two configurations ‘T’ and ‘R + T’ laminated double glazing system. Besides the obtained good agreement between the exact and estimated values, one can clearly see that the eigenfrequencies of the coupled system have increased when a rotational stiffness is added.

4.3. Eigenmodes shapes of the laminated double glazing system bonded by ‘R + T’ joint. In this section, the exact and estimated eigenmode shapes of the laminated double glazing system are presented and

| Mode | Translational stiffness 'T' | | | | | Translational + Rotational stiffness 'R + T' | | | | |
|------|-----------------------------|--------------------------|--------|--------|-----------|--|--------------------------|--------|--------|-----------|
| | Num. Efreq. (Hz) | Estim. Efreq. (Hz) | E_r | MAC | $E_f(\%)$ | Num. Efreq. (Hz) | Estim. Efreq. (Hz) | E_r | MAC | $E_f(\%)$ |
| 1 | 23.77 | 23 | 0.0095 | 0.7819 | 3.2394 | 37.18 | 37 | 0.0019 | 0.9976 | 0.4955 |
| 2 | 24.02 | 24 | 0.0263 | 0.8856 | 0.0833 | 37.81 | 38 | 0.0023 | 0.9994 | 0.4973 |
| 3 | 41.79 | 41.5 | 0.0019 | 0.9994 | 0.6939 | 57.27 | 57.5 | 0.0086 | 0.9913 | 0.3976 |
| 4 | 42.37 | 42.5 | 0.0006 | 0.9986 | 0.3068 | 58.21 | 58 | 0.0022 | 0.9969 | 0.3634 |
| 5 | 62.58 | 62.5 | 0.0163 | 0.8626 | 0.1278 | 84.69 | 84.5 | 0.0032 | 0.9963 | 0.2295 |
| 6 | 63.86 | 64 | 0.0001 | 1.0000 | 0.2192 | 88.28 | 88.5 | 0.0008 | 1.0000 | 0.2423 |
| 7 | 70.75 | 71 | 0.0053 | 0.9999 | 0.3534 | 90.15 | 90 | 0.0024 | 1.0000 | 0.1723 |
| 8 | 71.94 | 72 | 0.0025 | 0.9959 | 0.0834 | 91.96 | 92 | 0.0058 | 0.9883 | 0.0335 |
| 9 | 77.85 | 78 | 0.0061 | 0.9765 | 0.1927 | 101.77 | 102 | 0.0106 | 0.9602 | 0.2166 |
| 10 | 79.94 | 80 | 0.0022 | 1.0000 | 0.0751 | 105.34 | 105.5 | 0.0019 | 1.0000 | 0.1517 |
| 11 | 104.22 | 104 | 0.0037 | 0.9999 | 0.2111 | 131.66 | 131.5 | 0.0006 | 1.0000 | 0.1252 |
| 12 | 107.66 | 107.5 | 0.0058 | 0.9796 | 0.1486 | 135.52 | 135.5 | 0.0011 | 0.9995 | 0.0147 |
| 13 | 111.53 | 111.5 | 0.0102 | 0.6315 | 0.0269 | 135.76 | 136 | 0.0133 | 0.9035 | 0.1723 |
| 14 | 113.92 | 114 | 0.0025 | 0.9989 | 0.0702 | 139.91 | 140 | 0.0030 | 0.9989 | 0.0606 |
| 15 | 121.97 | 122 | 0.0319 | 0.8447 | 0.0246 | 148.74 | 149 | 0.0016 | 0.9997 | 0.1728 |
| 16 | 126.59 | 126.5 | 0.0267 | 0.1735 | 0.0711 | 162.01 | 162 | 0.0028 | 0.9949 | 0.0099 |
| 17 | 135.73 | 135.5 | 0.0093 | 0.9840 | 0.1695 | 166.09 | 166 | 0.0006 | 1.0000 | 0.0555 |
| 18 | 141.78 | 142 | 0.0011 | 0.9998 | 0.1552 | 175.49 | 175.5 | 0.0052 | 0.9965 | 0.0033 |
| 19 | 142.73 | 142.5 | 0.0018 | 0.9994 | 0.1611 | 177.83 | 178 | 0.0020 | 0.9994 | 0.0941 |
| 20 | 148.30 | 148.5 | 0.0026 | 0.9708 | 0.1349 | 180.59 | 180.5 | 0.0024 | 0.9962 | 0.0530 |
| 21 | 159.73 | 195.5 | 0.0057 | 0.9798 | 0.1440 | 193.38 | 193.5 | 0.0005 | 0.9999 | 0.0612 |
| 22 | 166.20 | 166 | 0.0003 | 1.0000 | 0.1203 | 196.62 | 196.5 | 0.0012 | 1.0000 | 0.0643 |
| 23 | 168.15 | 168 | 0.0037 | 0.9999 | 0.0892 | 204.28 | 204.5 | 0.0011 | 1.0000 | 0.1069 |
| 24 | 171.05 | 171 | 0.0033 | 0.9931 | 0.0292 | 205.99 | 206 | 0.0047 | 0.9922 | 0.0032 |
| 25 | 195.13 | 195 | 0.0959 | 0.1494 | 0.0666 | 222.30 | 222.5 | 0.0067 | 0.9841 | 0.0856 |
| 26 | 195.36 | 195.5 | 0.0046 | 0.9999 | 0.0717 | 234.47 | 234.5 | 0.0030 | 0.9999 | 0.0117 |
| 27 | 201.80 | 202 | 0.0011 | 1.0000 | 0.0991 | 238.18 | 238 | 0.0010 | 1.0000 | 0.0781 |
| 28 | 204.22 | 204 | 0.0426 | 0.4764 | 0.1077 | 242.95 | 243 | 0.0065 | 0.9850 | 0.0196 |
| 29 | 207.22 | 207 | 0.0675 | 0.0235 | 0.1062 | 243.33 | 243.5 | 0.0278 | 0.6943 | 0.0691 |
| 30 | 214.26 | 214.5 | 0.0385 | 0.7989 | 0.1120 | 248.59 | 248.5 | 0.0285 | 0.9056 | 0.0369 |
| 31 | 215.83 | 216 | 0.0421 | 0.8065 | 0.0788 | 259.04 | 259 | 0.0089 | 0.9902 | 0.4955 |
| 32 | 230.33 | 230.5 | 0.1840 | 0.8029 | 0.0738 | 265.25 | 265.5 | 0.0224 | 0.7569 | 0.4973 |

Table 3. Eigenfrequencies of the 'T' and 'R + T' coupled systems.

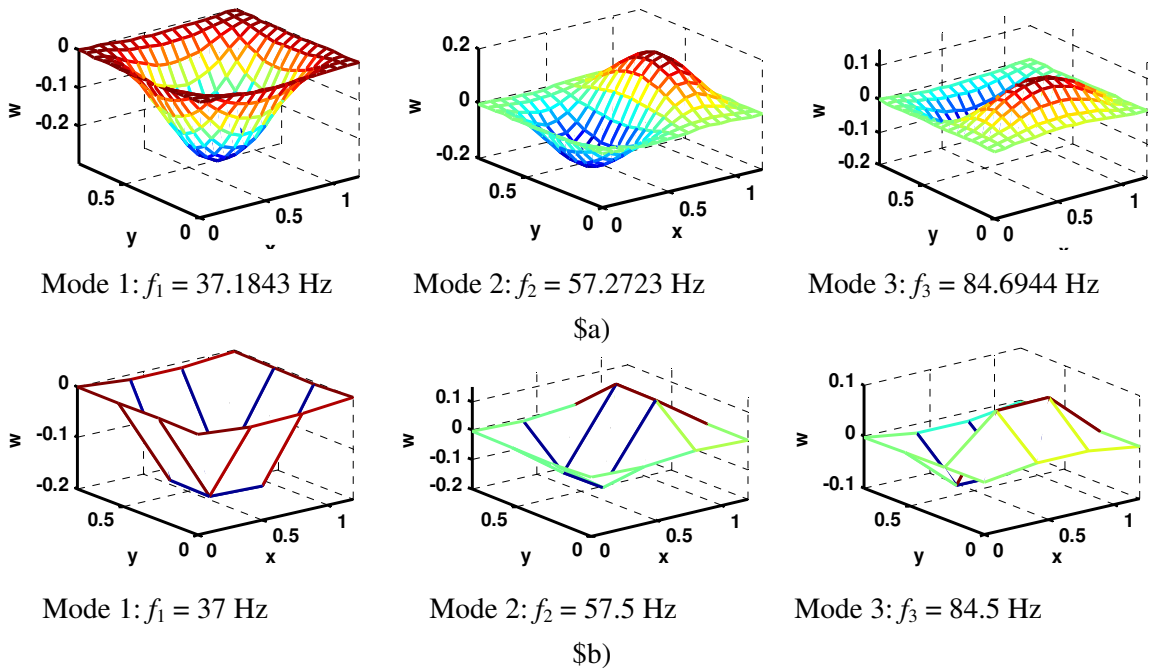


Figure 11. Eigenmode shapes of a laminated plate bonded by both translational and rotational joints. (a) Exact eigenmode shapes. (b) Estimated eigenmode shapes.

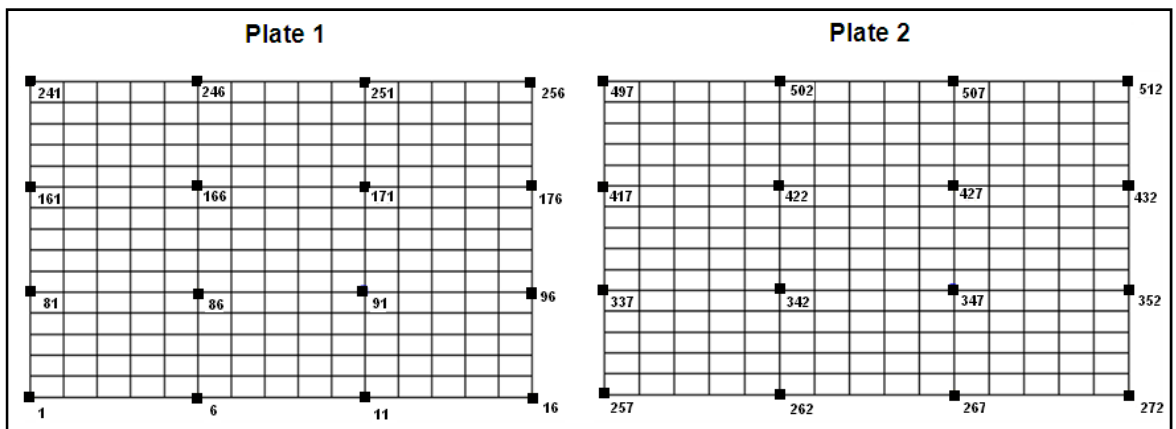


Figure 12. Coupled system vibratory response nodes.

commented. Consequently, the considered 32 coupled system vibratory response nodes let's to construct the investigated eigenmodes (Figures 17 and 18).

Here, four eigenmode shapes are estimated and presented and then, a good accord is obtained when comparing with numerical results. As discussed in [Basten et al. 2001; Akrouf et al. 2009; 2010], two categories of eigenfrequencies are found. The first one regroups those of a laminate alone bonded by 'R + T' joint. In this case, the two plates are vibrating in-phase. In fact, the middle joint doesn't generate a

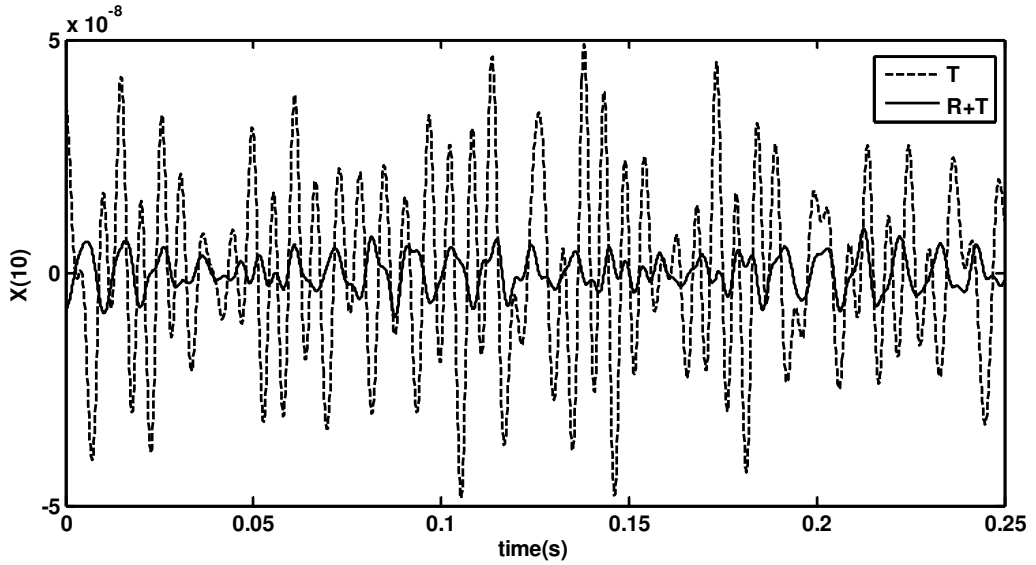


Figure 13. Observed signals of the first laminate at node 166.

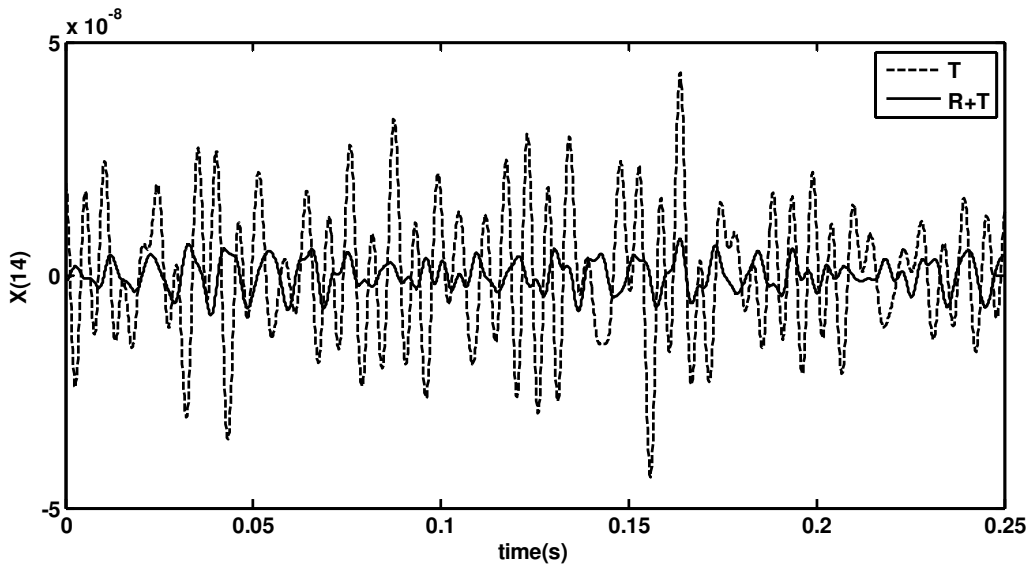


Figure 14. Observed signals of the first laminate at node 246.

coupling with laminates. The second category regroups the coupled eigenfrequencies which are affected by the coupling laminate-joint and where the two plates are vibrating in opposition.

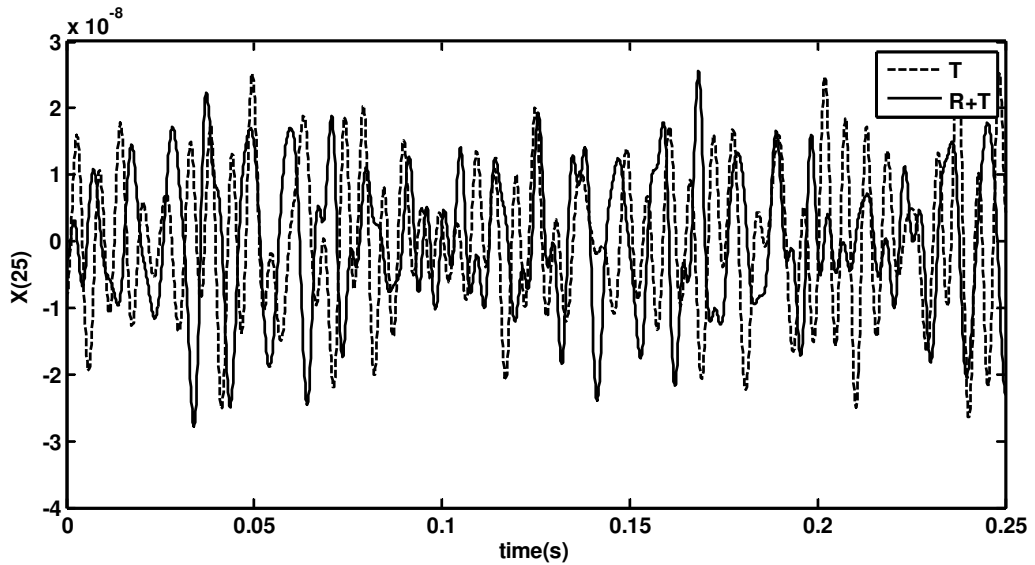


Figure 15. Observed signals of the second laminate at node 417.

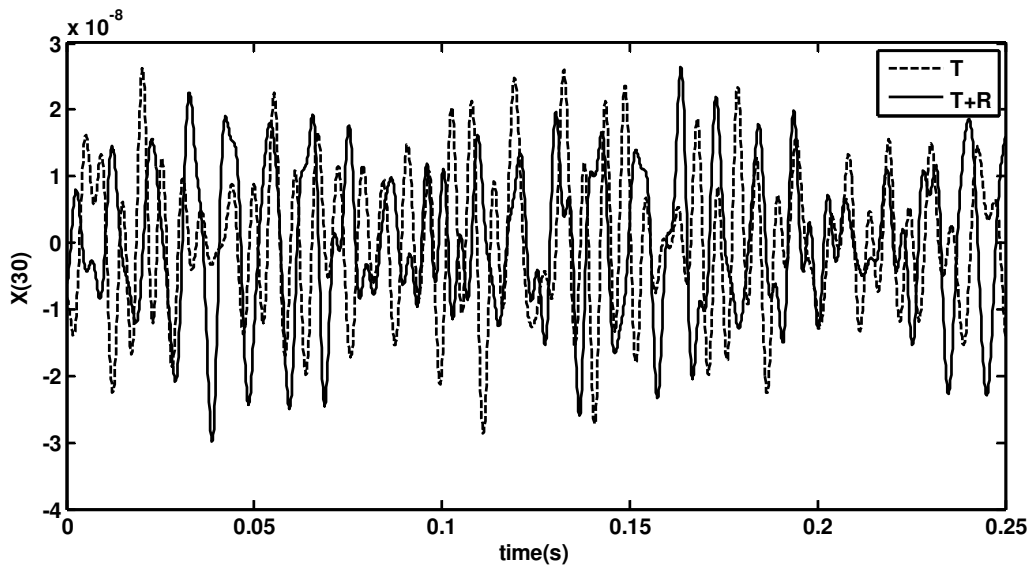


Figure 16. Observed signals of the second laminate at node 502.

5. Conclusion

In this work, the dynamic modal behavior of a thin-film laminated double glazing system is investigated. In this case, the edge stiffness boundary conditions associated to an elastic joint (translational and rotational effects) are modeled and its influence on a given structure (laminated plate alone or double glazing system) can be analyzed. For this purpose, the OMA method is presented and exploited in

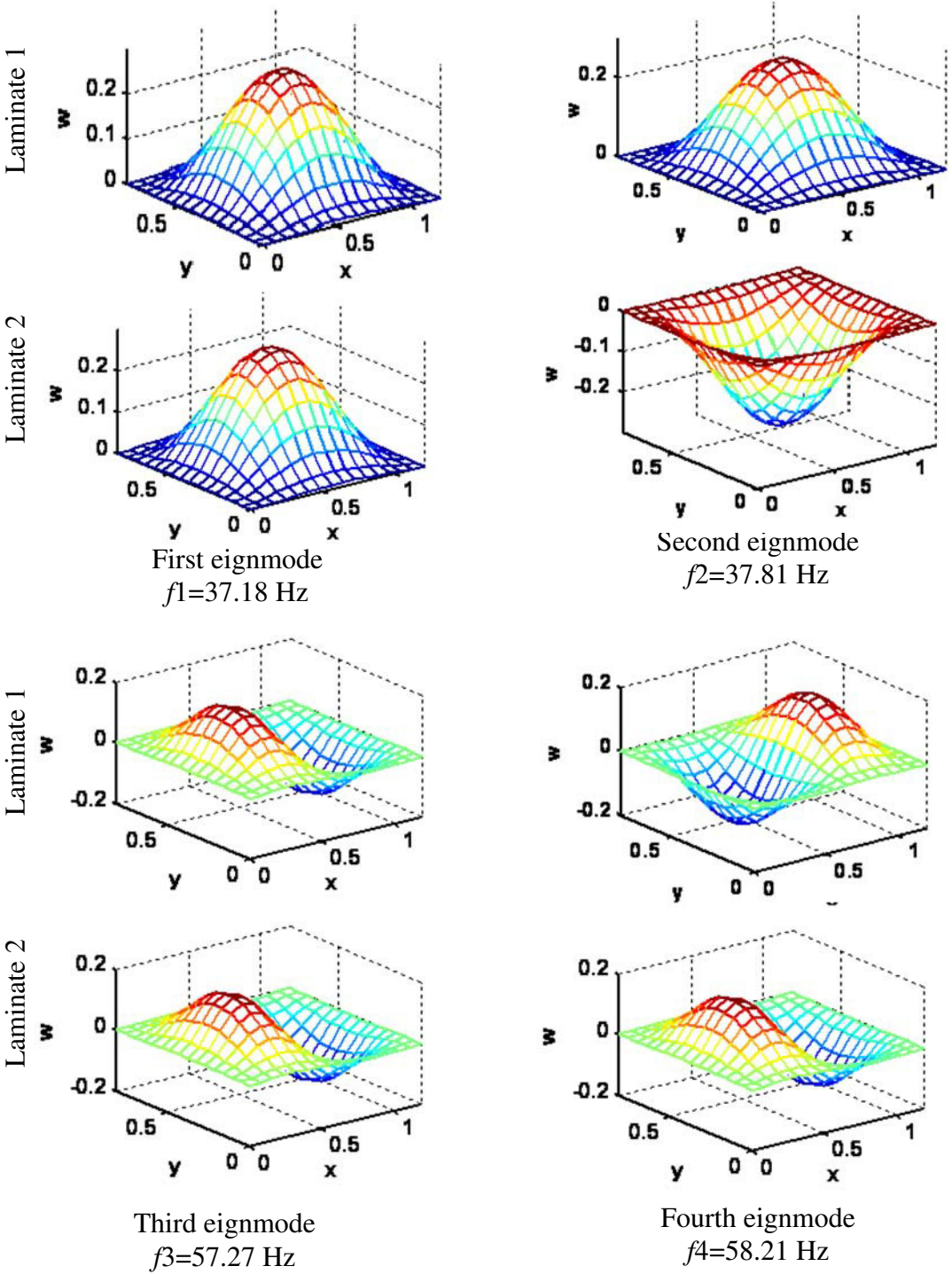


Figure 17. Exact eigenmodes shapes of the laminated double glazing system.

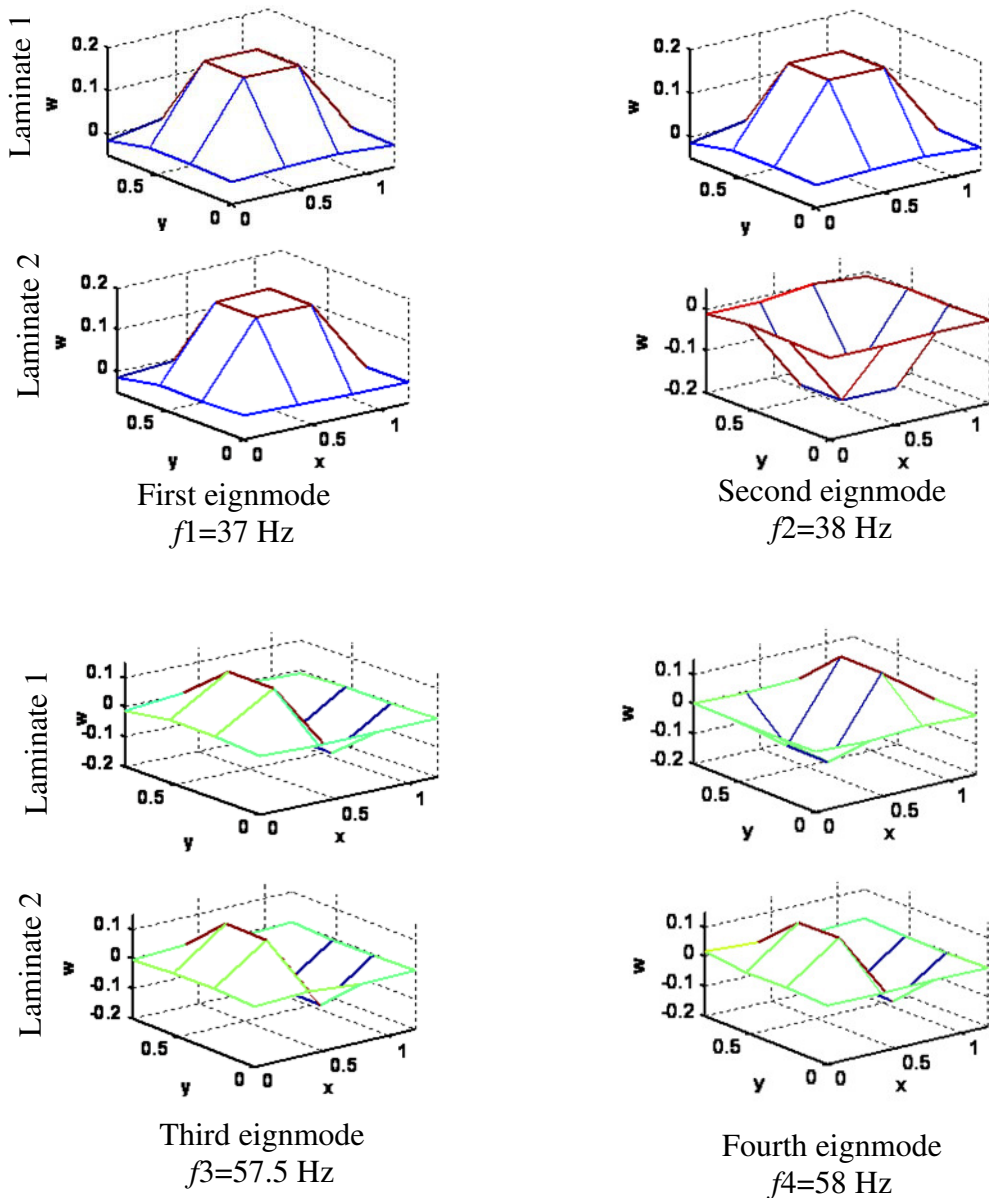


Figure 18. Estimated eigenmodes shapes of the laminated double glazing system.

order to determine the modal characteristics (eigenfrequencies and eigenmode shapes) of the coupled system. The modal procedure validation is based on the calculation of three performance criteria defined by the Modal Assurance Criterion (MAC), the approximation error of the eigenmode shapes (Er) and the relative error between numerical and estimated eigenfrequencies (Ef). Hence, a good agreement is achieved by comparing the exact (obtained by FE) and estimated (obtained by OMA) eigenmodes. Then, from the calculated results, it's deduced that when angular springs are added to linear springs at

the laminate's edges, the vibratory behavior of the studied system becomes much better. In fact, reduced vibration amplitudes are obtained and an improved rigidity can be conferred to the considered structure due to the increasing of its natural frequencies.

References

- [Abbès et al. 2011] M. S. Abbès, M. Miladi Chaabane, A. Akrou, T. Fakhfakh, and M. Haddar, “Vibratory behavior of a double panel system by the operational modal analysis”, *Int. J. Model. Simul. Sci. Comput.* **2**:4 (2011), 459–479.
- [Abdennadher et al. 2005a] M. Abdennadher, S. Fenina, L. Hammami, and M. Haddar, “Double glazing vibroacoustic behaviour”, *Electron. J. Tech. Acoust.* **6** (2005), 1–12.
- [Abdennadher et al. 2005b] M. Abdennadher, S. Fenina, L. Hammami, and M. Haddar, “Vibro-acoustic analysis of a double sandwich panels system”, *Int. J. Eng. Simul.* **6**:1 (2005), 3–9.
- [Akrou et al. 2008a] A. Akrou, L. Hammami, M. Ben Tahar, and M. Haddar, “Inter-facial shear effects of ultra-thin film on laminated glass plate dynamical behaviour”, *Proc. Inst. Mech. Eng. C, J. Mech. Eng. Sci.* **222**:8 (2008), 1421–1433.
- [Akrou et al. 2008b] A. Akrou, C. Karra, L. Hammami, and M. Haddar, “Viscothermal fluid effects on vibro-acoustic behaviour of double elastic panels”, *Int. J. Mech. Sci.* **50**:4 (2008), 764–773.
- [Akrou et al. 2009] A. Akrou, L. Hammami, M. Ben Tahar, and M. Haddar, “Vibro-acoustic behaviour of laminated double glazing enclosing a viscothermal fluid cavity”, *Appl. Acoust.* **70**:1 (2009), 82–96.
- [Akrou et al. 2010] A. Akrou, L. Hammami, C. Karra, M. Ben Tahar, and M. Haddar, “Vibro-acoustic damping simulation of two laminated glass panels coupled to viscothermal fluid layer”, *Int. J. Acoust. Vib.* **15**:2 (2010), 79–90.
- [Antoni 2005] J. Antoni, “Blind separation of vibration components: principles and demonstration”, *Mech. Syst. Signal Process.* **19**:6 (2005), 1166–1180.
- [Antoni et al. 2004] J. Antoni, L. Garibaldi, S. Marchesiello, and M. Sidahmed, “New separation techniques for output-only modal analysis”, *Shock Vib.* **11**:3 (2004), 227–242.
- [Antonio et al. 2003] J. M. P. Antonio, A. Tadeu, and L. Godinho, “Analytical evaluation of the acoustic insulation provided by double infinite walls”, *J. Sound Vib.* **263**:1 (2003), 113–29.
- [Assaf 1991] S. Assaf, *Modélisation par la méthode des éléments finis du comportement vibratoire des poutres et plaques sandwichs: métal matériaux viscoélastiques*, Ph.D. thesis, University of Technology of Compiègne, Compiègne, 1991.
- [Basten et al. 2001] T. G. H. Basten, P. J. M. van der Hoogt, R. M. E. J. Spiering, and H. Tijdeman, “On the acousto-elastic behaviour of double-wall panels with a viscothermal air layer”, *J. Sound Vib.* **243**:4 (2001), 699–719.
- [Bouhioü 1993] H. Bouhioü, *Étude vibro-acoustique d'un montage en double parois de verre*, Ph.D. thesis, University of Technology of Compiègne, Compiègne, 1993.
- [Carrera 2004] E. Carrera, “On the use of Murakami's zig-zag function in the modeling of layered plates and shells”, *Comput. Struct.* **82** (2004), 541–554.
- [Cheng et al. 2005] L. Cheng, Y. Y. Li, and J. X. Gao, “Energy transmission in a mechanically linked double-wall structure coupled to an acoustic enclosure”, *J. Acoust. Soc. Am.* **117**:5 (2005), 2742–51.
- [Héroult and Ans 1984] J. Héroult and B. Ans, “Réseaux de neurones à synapses modifiables: décodage de messages sensoriels composites par un apprentissage non supervisé et permanent”, *C. R. Acad. Sci. III Sci. Vie* **209**:13 (1984), 525–528.
- [Héroult et al. 1985] J. Héroult, C. Jutten, and B. Ans, “Détection de grandeurs primitives dans un message composite par une architecture de calcul neuromimétique en apprentissage non supervisé”, pp. 1017–1022 in *Dixième Colloque sur le Traitement du Signal et ses Applications* (Nice, 1985), Groupe de Recherche et d'Étude de Traitement du Signal et des Images, Gif-sur-Yvette, 1985.
- [Kerschen et al. 2007] G. Kerschen, F. Poncelet, and J.-C. Golinval, “Physical interpretation of independent component analysis in structural dynamics”, *Mech. Syst. Signal Process.* **21** (2007), 1561–1575.
- [Khdeir and Reddy 1999] A. A. Khdeir and J. N. Reddy, “Free vibrations of laminate composite plate using second-order shear deformation theory”, *Comput. Struct.* **71** (1999), 617–626.

- [Nguyen et al. 1994] H. L. Nguyen, J. Caelen, and C. Jutten, “Réhaussement de la parole par la séparation de sources dans un mélange convolutif”, *J. Phys. (France) IV* **4**:C5 (1994), 541–544.
- [Park et al. 2003] J. Park, L. Mongeau, and T. Siegmund, “Influence of support properties on the sound radiated from the vibrations of rectangular plates”, *J. Sound Vib.* **264** (2003), 775–794.
- [Poncelet et al. 2007] F. Poncelet, G. Kerschen, J.-C. Golinval, and D. Verhelst, “Output-only modal analysis using blind source separation techniques”, *Mech. Syst. Signal Process.* **21** (2007), 2335–2358.
- [Reddy 1997] J. N. Reddy, *Mechanics of laminated composite plates: theory and analysis*, CRC, Boca Raton, FL, 1997.
- [Vallaban et al. 1997] C. V. G. Vallaban, M. Z. Asik, and K. Kandil, “Analysis of structural glazing systems”, *Comput. Struct.* **65** (1997), 231–239.
- [Zarzoso and Comon 2008] V. Zarzoso and P. Comon, “Robust independent component analysis for blind source separation and extraction with application in electrocardiography”, pp. 3344–3347 in *Personalized healthcare through technology: proceedings of the 30th Annual International of the IEEE Engineering in Medicine and Biology Society* (Vancouver, BC, 2008), IEEE, Piscataway, NJ, 2008.
- [Zenkert 1995] D. Zenkert, *An introduction to sandwich construction*, Engineering Materials Advisory Services, London, 1995.
- [Zhou and Chelidze 2007] W. Zhou and D. Chelidze, “Blind source separation based vibration mode identification”, *Mech. Syst. Signal Process.* **21** (2007), 3072–3087.

Received 5 Jun 2012. Revised 3 Oct 2012. Accepted 16 Oct 2012.

ALI AKROUT: ali.akrout@enit.rnu.tn

Mechanical Engineering Department, National School of Engineers of Sfax, Unit of Mechanics, Modelling and Manufacturing (U2MP), BP. 1173, 3038 Sfax, Tunisia

MARIEM MILADI CHAABANE: mariam.mi@hotmail.fr

Mechanical Engineering Department, National School of Engineers of Sfax, Unit of Mechanics, Modelling and Manufacturing (U2MP), BP. 1173, 3038 Sfax, Tunisia

LOTFI HAMMAMI: lotfi.hammami@enis.rnu.tn

Mechanical Engineering Department, National School of Engineers of Sfax, Unit of Mechanics, Modelling and Manufacturing (U2MP), BP. 1173, 3038 Sfax, Tunisia

MOHAMED HADDAR: mohamed.haddar@enis.rnu.tn

Mechanical Engineering Departement, National Engineering School of Sfax, Unit of Mechanics, Modelling and Manufacturing (U2MP), BP. 1173, 3038 Sfax, Tunisia

JOURNAL OF MECHANICS OF MATERIALS AND STRUCTURES

jomms.net

Founded by Charles R. Steele and Marie-Louise Steele

EDITORS

CHARLES R. STEELE Stanford University, USA
DAVIDE BIGONI University of Trento, Italy
IWONA JASIUK University of Illinois at Urbana-Champaign, USA
YASUHIRO SHINDO Tohoku University, Japan

EDITORIAL BOARD

H. D. BUI École Polytechnique, France
J. P. CARTER University of Sydney, Australia
R. M. CHRISTENSEN Stanford University, USA
G. M. L. GLADWELL University of Waterloo, Canada
D. H. HODGES Georgia Institute of Technology, USA
J. HUTCHINSON Harvard University, USA
C. HWU National Cheng Kung University, Taiwan
B. L. KARIHALOO University of Wales, UK
Y. Y. KIM Seoul National University, Republic of Korea
Z. MROZ Academy of Science, Poland
D. PAMPLONA Universidade Católica do Rio de Janeiro, Brazil
M. B. RUBIN Technion, Haifa, Israel
A. N. SHUPIKOV Ukrainian Academy of Sciences, Ukraine
T. TARNAI University Budapest, Hungary
F. Y. M. WAN University of California, Irvine, USA
P. WRIGGERS Universität Hannover, Germany
W. YANG Tsinghua University, China
F. ZIEGLER Technische Universität Wien, Austria

PRODUCTION production@msp.org

SILVIO LEVY Scientific Editor

Cover design: Alex Scorpan

See <http://jomms.net> for submission guidelines.

JoMMS (ISSN 1559-3959) is published in 10 issues a year. The subscription price for 2012 is US\$555/year for the electronic version, and \$735/year (+ \$60 shipping outside the US) for print and electronic. Subscriptions, requests for back issues, and changes of address should be sent to Mathematical Sciences Publishers, Department of Mathematics, University of California, Berkeley, CA 94720–3840.

JoMMS peer-review and production is managed by EditFLOW[®] from Mathematical Sciences Publishers.

PUBLISHED BY
 **mathematical sciences publishers**
<http://msp.org/>

A NON-PROFIT CORPORATION

Typeset in L^AT_EX

Copyright ©2012 by Mathematical Sciences Publishers

Journal of Mechanics of Materials and Structures

Volume 7, No. 8-9

October 2012

- A model for the shear displacement distribution of a flow line in the adiabatic shear band based on gradient-dependent plasticity**
XUE-BIN WANG and BING MA 735
- A pull-out model for perfectly bonded carbon nanotube in polymer composites**
KHONDAKER SAKIL AHMED and ANG KOK KENG 753
- A perfectly matched layer for peridynamics in two dimensions**
RAYMOND A. WILDMAN and GEORGE A. GAZONAS 765
- Displacement field in an elastic solid with mode-III crack and first-order surface effects**
TAMRAN H. LENGYEL and PETER SCHIAVONE 783
- On the choice of functions spaces in the limit analysis for masonry bodies**
MASSIMILIANO LUCCHESI, MIROSLAV ŠILHAVÝ and NICOLA ZANI 795
- Edge stiffness effects on thin-film laminated double glazing system dynamical behavior by the operational modal analysis**
ALI AKROUT, MARIEM MILADI CHAABANE, LOTFI HAMMAMI and MOHAMED HADDAR 837
- Network evolution model of anisotropic stress softening in filled rubber-like materials**
ROOZBEH DARGAZANY, VU NGOC KHIÊM, UWE NAVRATH and MIKHAIL ITSKOV 861